Limnol. Oceanogr., 37(3), 1992, 491–500

Self-shading of in-water optical instruments

Howard R. Gordon and Kuiyuan Ding
Department of Physics, University of Miami, Coral Gables, Florida 33124

Abstract

The self-shading of in-water optical radiometers for measuring upwelling radiance (L_u) and irradiance (E_u) is estimated from Monte Carlo simulations of the light field in the presence and absence of the instrument. It is found that the error (ϵ) induced by the presence of the radiometer is a function of its size and the *absorption* coefficient (a) of the medium, i.e. when $\epsilon \lesssim 15$–20% the error is independent of the scattering coefficient (b). Direct measurement of L_u or E_u with $\epsilon \leq 5\%$ places severe limitations on the instrument size, e.g. in the case of a cylindrical housing and small solar zenith angles (the worst case) the diameter of the instrument must be $\lesssim 1/30a$ for E_u and $\lesssim 1/100a$ for L_u. A correction method based on a simple model of ϵ is proposed and it is shown that when used these constraints on the diameter are reduced to $\lesssim 1/6a$ and $\lesssim 1/30a$, respectively, for an after-correction error of 5%. The self-shading error is estimated across the spectrum as a function of the pigment concentration of case 1 waters, and it is found that it can be large for typical radiometers, especially at high pigment concentrations or wavelengths >600 nm.

The next generation of ocean color sensors, such as SeaWiFS (NASA 1987) will have radiometric sensitivities (through increased signal-to-noise and finer resolution intervals) superior to the Coastal Zone Color Scanner (CZCS) (Gordon et al. 1980; Hovis et al. 1980). They also will be equipped with additional spectral bands, e.g. a band near 400 nm to separate the detrital and viable phytoplankton signals, and near-infrared (NIR) bands at 765 and 865 nm to aid in atmospheric correction. The rationale for the NIR bands is that a negligible amount of radiance will exit the ocean at these wavelengths, and this allows an assessment of the properties of the atmosphere required for removal of its "noise" (Gordon et al. 1983; Gordon and Morel 1983). In case 1 oceanic waters (Morel and Prieur 1977) during intense phytoplankton bloom conditions or case 2 coastal waters, however, the water-leaving radiance in these bands will no longer be negligible. Thus, in preparation for these new ocean color systems, there is interest in measuring the water-leaving radiance, or the upwelling radiance just beneath the surface (L_u) (units given in list of notation), and the upwelling irradiance (E_u) in the NIR as a function of the concentration of the constituents of the water—pigments and seston load.

The very large absorption coefficients in the NIR, e.g. the absorption coefficient of pure water being 2.5 and 5.1 m^{-1} at 765 and 865 nm (Hale and Querry 1973), means that the perturbation of the in-water light field by the presence of the sensor, and in particular its housing, can produce a significant error in measurement. For example, if the size of the instrument housing is of the order of the absorption coefficient (a) of the medium, it is likely that a significant portion of the medium that is accessible to the sensor, considering its field of view and absorption, is in the shadow of the housing, i.e. not exposed to direct sunlight.

In this paper we use Monte Carlo radiative transfer simulations to quantify the magnitude of the error induced by this self-shading and show that without corrections it can be reduced to manageable limits in the NIR only by utilizing instruments whose size is a small fraction of the absorption length $1/a$. A correction scheme is proposed that can relax this constraint significantly.

Radiance in the ocean is governed by the radiative transfer equation (RTE). Typically, for studies of the in-water light field, it is assumed that either the ocean is homogeneous or its optical properties depend only on depth (not on horizontal position). Furthermore, illumination of the sea from the

Acknowledgments

This work received support from the Office of Naval Research Ocean Optics Program under grant N00014-89-J-1985 and from the National Aeronautics and Space Administration under contract NAS5-30911 and grant NAGW-273.

Notation

a	Absorption coefficient, m^{-1}
b	Scattering coefficient, m^{-1}
$\beta(\alpha)$	Volume scattering function, m^{-1} $ster^{-1}$
c	Attenuation coefficient ($a + b$), m^{-1}
C	Pigment concentration, mg m^{-3}
D	Diameter of the sensor housing, m
D_{max}	Maximum D for a given ϵ, m
ϵ	Relative error in L_u or E_u
E_u, E_d	Upwelling and downwelling irradiance at $z = 0$, mW cm^{-2} μm^{-1}
K_u	Upwelling and downwelling radiance attenuation coefficient, m^{-1}
K(PAR)	Attenuation coefficient for PAR, m^{-1}
L_u	Upwelling radiance at $z = 0$, mW cm^{-2} μm^{-1} $ster^{-1}$
R	Radius of the sensor housing, m
θ_0	Solar zenith angle, degrees
θ_{0w}	Solar zenith angle in the water, degrees
ω_0	Single scattering albedo (b/c)
z	Depth, m

sun and sky is assumed to be independent of horizontal position. Under these conditions, the RTE is greatly simplified and radiance is independent of horizontal position, depending only on depth and viewing direction. The RTE and some properties of its (numerical) solutions obtained in such oceans are provided by Gordon (1989). For the present study, however, although the ocean is assumed to be homogeneous, the presence of the instrument destroys the horizontal translational invariance of the solution and the full dependence of the radiance on position (vertical and horizontal) must be determined.

The light field is governed by the inherent optical properties (Preisendorfer 1961) of the medium, the beam attenuation coefficient (c), and the volume scattering function, [$\beta(\alpha)$] (i.e. the differential scattering cross-section per unit of volume). The beam attenuation coefficient is related to the absorption (a) and scattering (b) coefficients through $c = a + b$. Two auxiliary optical properties that are widely used in radiative transfer theory are the scattering phase function $P = \beta/b$ and the single-scattering albedo or photon survival probability $\omega_0 = b/c$. In the results presented here, the scattering phase function used for the medium is identical to "KA" used by Gordon et al. (1975) and corresponds to measurements made by Kullenberg (1968) in the Sargasso Sea in the red (632.8 nm). This phase function is believed to be appropriate because we are most interested in the red-NIR portions of the spectrum; we shall demonstrate later, however, that our results are not particularly sensitive to scattering and hence should be nearly independent of the scattering phase function.

In the simulations the instrument is imagined to be a circular disk of radius R floating just beneath the sea surface. The sensor itself is treated initially as a *point* at the center of the disk (Fig. 1). The disk represents the housing of the instrument which, when illuminated by solar irradiance, casts a refracted shadow as shown in Fig. 1. In reality, the instrument housing would more likely be a cylinder, which would cast an even larger shadow, so the results that we present must *underestimate* the influence of the instrument. This larger shadow will be farther removed from the sensor, however, and will have only a minor effect when the absorption coefficient of the medium is large, particularly in the case of L_u. The sensor, as shown in Fig. 1, measures the radiance L_u with a finite field of view; in our simulations, the field of view is infinitesimal. Simulations are also carried out in which the sensor measures upwelling irradiance, E_u (i.e. has a 2π field of view).

Initially, in both simulations the incident irradiance is from the sun only. The contribution to L_u and E_u from skylight incident on the sea surface can be neglected for wavelengths >600 nm, because it should not exceed 10% of the total in this spectral range. To apply the results to wavelengths <600 nm, however, we must also determine the influence of skylight, and this application is effected with the aid of a simplified model of skylight. The solution of the radiative transfer equation is carried out utilizing the backward Monte Carlo technique with correlated sampling. It is the same computer code used to estimate the perturbation of the in-water light field due to the presence of a ship on the sea surface (Gordon 1985). The code was modified *only* to accommodate the assumed shape of the sensor, which replaces the ship (i.e. Fig. 1). A detailed discussion of the method is provided by Gordon (1985).

In the situation depicted in Fig. 1, it is

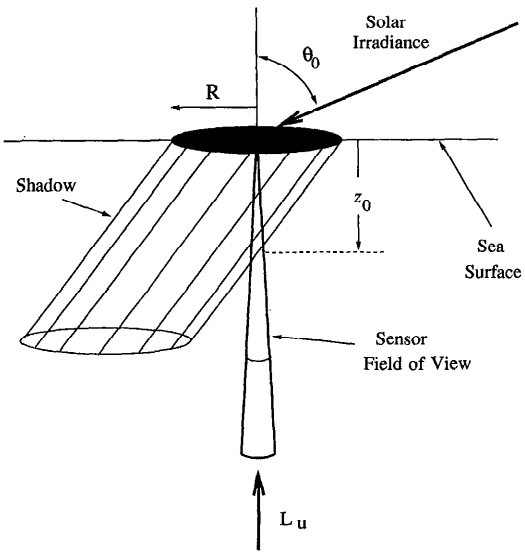

Fig. 1. Schematic of the geometry of the simulations for a point sensor.

easy to show that for a given θ_0 the measured radiance depends on c and R only through the product cR. Thus, in the computations R is fixed at 1 m and c varies from 0.01 to 30 m^{-1}. Given c and the scattering phase function, the optical properties of the water are determined by specifying ω_0. Error ϵ (in %) in the measured value of L_u just beneath the surface as a function of cR is estimated (Fig. 2) for $\omega_0 = 0.5$, 0.7, 0.9, and 0.95. ϵ is defined by

$$\epsilon \equiv \frac{L_u^{\text{true}} - L_u^{\text{measured}}}{L_u^{\text{true}}}. \qquad (1)$$

Notice (Fig. 2) that the range of the error in Eq. 1 is from 0 to 100%; when the error is near 100%, however, L_u^{measured} is only a small fraction of L_u^{true}. Recalling that multiple scattering increases with ω_0 (the fraction of c due to scattering), one would expect that, for a given c, as ω_0 increases the shadowed region in Fig. 1 would fill in with light and the error would become smaller. Figure 2 seems to confirm this expectation. When $cR = 1$ the error decreases from ~90% to ~25% as ω_0 increases from 0.5 to 0.95.

When the computations in Fig. 2 are plotted as a function of aR rather than cR (Fig. 3) the errors fall on what appears to be a "universal" curve in which they are approximately independent of ω_0. In fact, the dependence on ω_0 progressively weakens as the solar zenith angle increases (Figs. 3, 4). Also, when the error is small, there is virtually *no* dependence of the error on ω_0, suggesting that it should be possible to model the $aR \ll 1$ portion of the curves in Figs. 3 and 4 by ignoring scattering completely. To do so we assume that in the absence of the instrument $L_u^{\text{true}}(z) = L_u^{\text{true}}(0) \exp(-K_u z)$, where K_u is the upwelling radiance attenuation coefficient and z is depth. (Note that there must be *some* scattering because this phenomenon is the origin of L_u, so we are really assuming only that $\omega_0 \ll 1$, i.e. $b \ll a$.) Let z_0 be the depth at which the sensor field of view leaves the instrument shadow as shown in Fig. 1. Then,

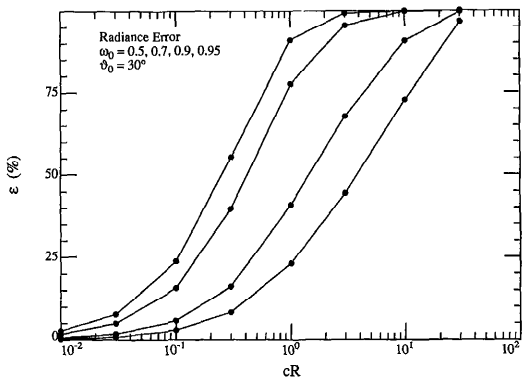

Fig. 2. Error in L_u defined in Eq. 1 as a function of cR. The curves from left to right correspond to increasing values of ω_0 from 0.5 to 0.95. The lines simply connect the points to separate the various values of ω_0. $\theta_0 = 30°$.

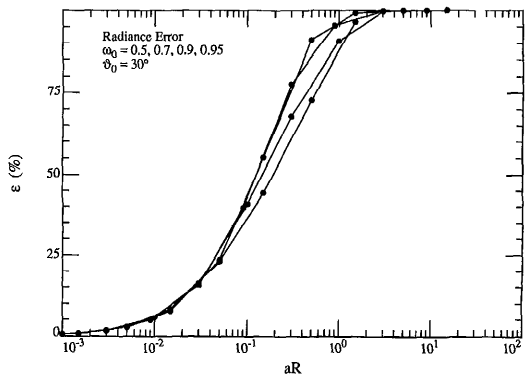

Fig. 3. Error in L_u defined in Eq. 1 taken from Fig. 2 and replotted as a function of aR rather than cR.

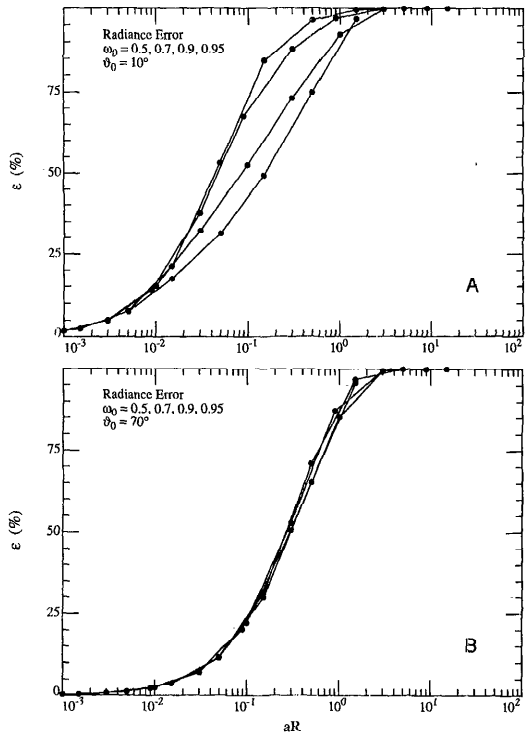

Fig. 4. As Fig. 3, except (A) $\theta_0 = 10°$ and (B) $\theta_0 = 70°$.

$z_0 = R/\tan\theta_{0w}$, where θ_{0w} is the refracted solar zenith angle given by Snell's law: $m_w \sin\theta_{0w} = \sin\theta_0$, with $m_w = 1.338$. Now, because of the absence of direct sunlight, there is no upwelled radiance added to L_u between z_0 and the surface, so $L_u^{\text{measured}}(0) = L_u^{\text{true}}(z_0)\exp(-az_0)$ where we have used the assumption that $b \ll a$. Combining, we have $L_u^{\text{measured}}(0) = L_u^{\text{true}}(0)\exp[-(a + K_u)z_0]$, or $L_u^{\text{measured}}(0) \approx L_u^{\text{true}}(0)\exp[-2az_0]$ where K_u is approximated by a. Thus, the error in Eq. 1 is

$$\epsilon = [1 - \exp(-kaR)] \qquad (2)$$

where $k = 2/\tan\theta_{0w}$. The Monte Carlo simulations (Fig. 3) clearly fit Eq. 2 well for $aR \lesssim 0.1$ (Fig. 5), and Eq. 2 also describes the general shape of the curve. Deviations from the model are due only to scattering and thus represent a true filling in of the geometrical shadow in Fig. 1 with light. For smaller values of θ_0 where the error is more strongly dependent on ω_0 (i.e. the filling in

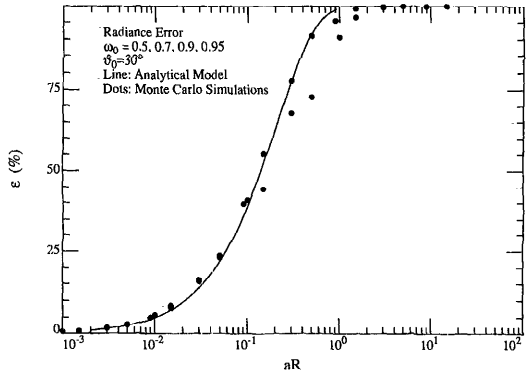

Fig. 5. Comparison between the Monte Carlo simulations of the error in L_u for the same simulations as in Fig. 3 with the result of the analytical model.

of the geometrical shadow becomes important), the maximum of aR for which the analytical model applies is reduced: $aR \lesssim 0.01$ and 0.03 for $\theta_0 = 10°$ and 20°. When $\theta_0 = 0$, the analytical model breaks down and the error is found to be strongly dependent on ω_0 for all values of aR that we examined ($aR \geq 0.0005$).

Anticipating that the analytical model may be useful for providing a correction for the shadowing error (when it is small and therefore independent of ω_0), we have fitted ϵ for $aR \leq 0.1$ to Eq. 2 with k replaced by a variable k', itself determined by a least-squares analysis. The $k'\tan\theta_{0w}$ values are all reasonably close (within ~20%) to the value of 2 predicted by the analytical model (Table 1, point sensor). Simulations of the error in the upwelling irradiance E_u have also been carried out (Fig. 6). Error in E_u is similar to that of L_u; in the case of E_u, however, dependence of the error on ω_0 is very weak even for $\theta_0 = 0$. Although no analytical

Table 1. Values of $k'\tan\theta_{0w}$ derived by fitting the Monte Carlo results for the error in L_u to Eq. 2.

θ_0	Point sensor	Finite sensor
10°	2.17*	1.79*
20°	2.23†	1.83†
30°	2.23	1.76
40°	2.29	1.84
50°	2.37	1.92
60°	2.41	1.97
70°	2.45	2.01

* $aR \leq 0.01$.
† $aR \leq 0.03$.

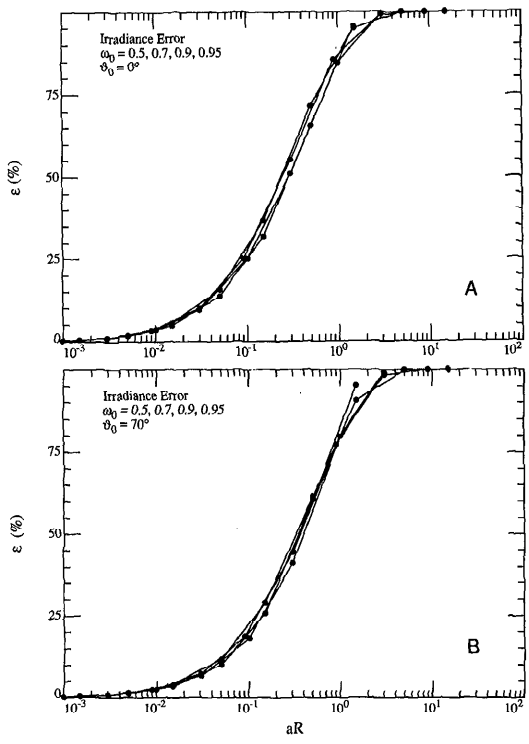

Fig. 6. Irradiance error as a function of aR for (A) $\theta_0 = 0°$ and (B) $\theta_0 = 70°$.

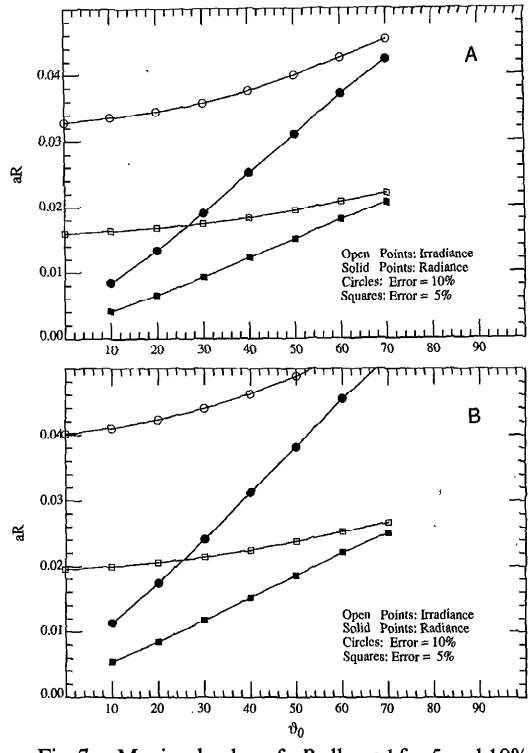

Fig. 7. Maximal value of aR allowed for 5 and 10% errors in L_u or E_u as a function of the sun angle for (A) a *point* sensor and (B) a *finite* sensor.

model for the irradiance error has been worked out, the similarity of the shapes of the curves in the figures for L_u and E_u suggest that for $aR \ll 1$ the E_u error should also fit Eq. 2 with k replaced by k' (cf. Table 2, point sensor). Unlike the error in L_u, the error in E_u is a very weak function of θ_0. (Recall that for L_u, $k' \sim 2/\tan \theta_{0w}$.)

As a guide for the design of instrumentation for measuring L_u and E_u, we have computed the value of aR that results in a 5% and 10% error in L_u or E_u (Fig. 7A). This guide used the fits of the Monte Carlo results to Eq. 2 for those simulations with $aR \leq 0.1$. The value of k' (Table 1) is used in place of k in Eq. 2 to estimate aR for a given error. Note that this procedure provides the *maximal* value of aR for a given error. As expected, in the case of E_u the maximum aR is only weakly dependent on θ_0 in contrast to a strong and almost linear dependence for L_u. The more striking aspect, however, is the very small values of aR required for measurements with errors no larger than ~5–10%. For example, in the least restrictive case (E_u and an error of 10% at $\theta_0 = 70°$) the maximal $aR < 1/20$ (i.e. the maximal *radius* of the instrument housing must be $\lesssim 1/20a$). For $\theta_0 = 0$ the corresponding value is $1/30a$. For a 5% error these values are halved, and direct measurement of E_u at 765 and 865 nm with an error of $\lesssim$5% for all values of θ_0 requires a sensor with a housing having a maximal *radius* of ~0.66 and 0.33 cm, respectively, assuming the absorption coefficient of pure water. For radiance, maximal radii are even

Table 2. Values of k' derived by fitting the Monte Carlo results for the error in E_u to Eq. 2.

θ_0	Point sensor	Finite sensor
10°	3.14	2.56
20°	3.05	2.49
30°	2.94	2.39
40°	2.80	2.28
50°	2.64	2.15
60°	2.47	2.03
70°	2.33	1.91

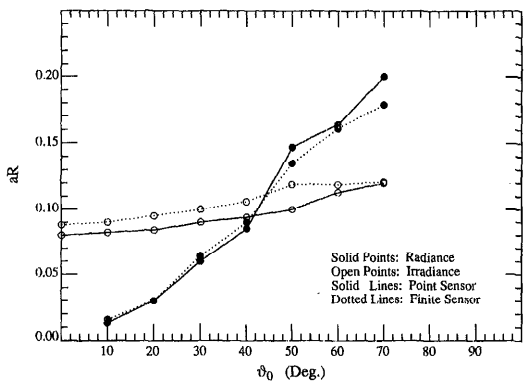

Fig. 8. Estimate of the maximal value of aR allowed for an error <5% in L_u or E_u for direct sunlight illumination when the self-shading correction method described in the text is applied. For skylight illumination, the maximal value of aR for L_u and E_u corresponds to the sunlight illumination case with $\theta_0 \sim 35°$ and 45°.

smaller and also depend strongly on the solar zenith angle, e.g. in the worst case (L_u and an error of 5% near $\theta_0 = 0$) the instrument radius must be $\lesssim 1/200a$.

For instruments with the design constraints described above, it is likely that the sensor will occupy a significant fraction of R. Thus, we have carried out additional simulations in which the sensor itself occupies the *entire* base of the instrument (i.e. has a radius R). For them, L_u and E_u errors are qualitatively similar to those for the point detector. An analysis of the error using Eq. 2, in a manner similar to that for the point detector above, for the finite sensor yields the values of $k'\tan\theta_{0w}$ and k' (Tables 1 and 2, finite sensor). Using these values of k', values of aR for 5 and 10% errors in L_u and E_u for the finite sensor have been computed (Fig. 7B). Only a small relaxation (~20%) of the constraint on aR with the larger sensor (Fig. 7A vs. 7B).

It is important to note that instruments may be larger than suggested in Fig. 7, if the shadowing error can be corrected. Such a correction can be made if the radiance or irradiance errors are sufficiently small and independent of ω_0. In this case, the error can be described by Eq. 2 with k replaced by k' in Table 1 or 2 and can be estimated accurately, *and corrected,* on the basis of aR alone. If aR is too large, however, corrections for self-shading cannot be made without knowing all of the inherent optical properties of the medium under study.

For a given desired accuracy for L_u^{true} (or E_u^{true}), it is possible to estimate the maximal allowed value of aR such that the shading correction can be made. To do so, we rewrite Eq. 1

$$L_u^{\text{true}} = \frac{L_u^{\text{measured}}}{1 - \epsilon}.$$

This form is used to correct the measured L_u for shading. Using Eq. 2 (with k replaced by k' in Table 1) to estimate ϵ will result, however, in an error $\Delta\epsilon$. This error produces an error in the retrieved of L_u^{true} given by

$$\frac{\Delta L_u^{\text{true}}}{L_u^{\text{true}}} = \frac{\Delta\epsilon}{1 - \epsilon}$$

(i.e. the error in retrieved value of L_u^{true} equals the % error in ϵ divided by $1 - \epsilon$). The $1 - \epsilon$ factor underscores the necessity for ϵ to be small to make a good correction.

For each of our simulations, we have determined $\Delta\epsilon/(1 - \epsilon)$ by comparing the value of ϵ derived from Eq. 2 with k' from Table 1 to that directly determined in the Monte Carlo simulation. For a desired accuracy of 5% in L_u (or E_u) the maximal value of aR allowed in order to achieve it was *estimated.* It could not be precisely determined because the computations were much too sparse in $aR - \omega_0$ space. This estimate (Fig. 8) may be ~10–15% too low for L_u and E_u. Note that aR for E_u is significantly larger than for L_u at small sun angles, which reflects the fact that E_u has less dependence on ω_0 for small θ_0. In contrast, the situation is reversed for large θ_0, as a comparison of Figs. 4B and 6B would suggest. Comparing Figs. 7A and 8 shows that a significant reduction in the constraint on aR (a factor of 4–15 depending on θ_0, when skylight can be ignored) can result from using the correction method described above.

Since our interest has centered on the NIR portion of the spectrum, skylight has been ignored in the computation thus far. We now investigate the effect of skylight by assuming that the sky radiance incident on the sea surface is independent of direction (uniform radiance distribution). Note that this model is also reasonable for completely

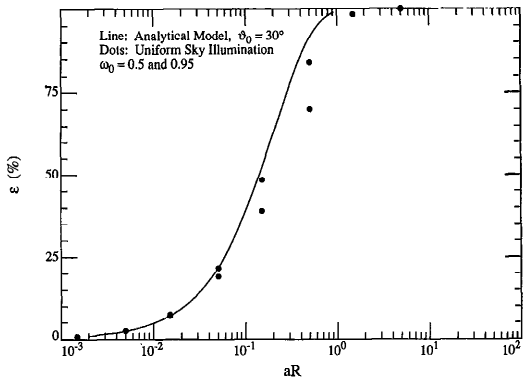

Fig. 9. Monte Carlo simulations (●) of the error in L_u defined in Eq. 1 as a function of aR compared with the analytical model (Eq. 2) with $\theta_0 = 30°$ (line). Incident illumination is from a sky of uniform radiance.

overcast conditions. In our Monte Carlo simulations the computed radiances $L_u(\theta_0)$ and irradiances $E_u(\theta_0)$ are normalized to a unit of irradiance from the sun on the *horizontal* sea surface, i.e. $E_d(\text{sun}) = F_0 \cos\theta_0$, where F_0 is the irradiance on a plane *normal* to the solar beam. If we assume that the sky provides uniform radiance, the upwelling radiance $L_u(\text{sky})$ and the irradiance $E_u(\text{sky})$ just beneath the sea surface are given by

$$L_u(\text{sky}) = \int_0^{\pi/2} L_u(\theta_0)\sin(2\theta_0)\, d\theta_0$$

and

$$E_u(\text{sky}) = \int_0^{\pi/2} E_u(\theta_0)\sin(2\theta_0)\, d\theta_0$$

where $L_u(\text{sky})$ and $E_u(\text{sky})$ are normalized to $E_d(\text{sky})$, the downwelling irradiance from the sky at the sea surface. Thus, we can compute the error in the case of skylight-only illumination by replacing L_u in Eq. 1 by $L_u(\text{sky})$ or $E_u(\text{sky})$ (cf. Fig. 9 for $\omega_0 = 0.5$ and 0.95—the extremes of our simulation set).

This analysis shows that the L_u error in the case of uniform sky illumination also becomes independent of scattering for sufficiently small aR (e.g. $aR \lesssim 0.05$) and that it can be computed accurately from Eq. 2 with $\theta_0 \approx 30°$ in the small-aR regime. Similar computations have been carried out for $E_u(\text{sky})$ for a point sensor, and for $L_u(\text{sky})$ and $E_u(\text{sky})$ for a finite sensor. For them,

Table 3. Values of k' derived by fitting the Monte Carlo results for the error in $L_u(\text{sky})$ and $E_u(\text{sky})$ to Eq. 2.

Quantity	Point sensor	Finite sensor
$L_u(\text{sky})$	4.61	3.74
$E_u(\text{sky})$	2.70	2.22

the error has been fitted to Eq. 2 with k replaced by k', and k' determined (Table 3) in a manner similar to the case of direct sunlight (Tables 1 and 2). The values of k' in Table 3 can be used directly to estimate the error for completely overcast conditions.

Except in cases of complete overcast, the sea surface receives irradiance from both the sun and sky. Under such illumination, the error in L_u is

$$\epsilon = \frac{\epsilon(\text{sun}) + \epsilon(\text{sky}) \times \text{ratio}}{1 + \text{ratio}} \qquad (3)$$

where

$$\text{ratio} = \frac{E_d(\text{sky})}{E_d(\text{sun})} \times \frac{L_u{}^{\text{true}}(\text{sky})}{L_u{}^{\text{true}}(\text{sun})},$$

$\epsilon(\text{sun})$ and $\epsilon(\text{sky})$ are the errors for illumination solely from the sun and sky, and $E_d(\text{sun})$ and $E_d(\text{sky})$ are the irradiances on the surface from the sun and sky. Note that our $L_u{}^{\text{true}}$ is normalized to unit irradiance E_d on the sea surface, so $E_d L_u{}^{\text{true}}$ is the actual upwelling radiance that would be observed with an instrument casting no shadow. A similar equation can be written for the error in E_u.

To utilize Eq. 3 it is necessary to know $L_u{}^{\text{true}}(\text{sky})/L_u{}^{\text{true}}(\text{sun})$. Over most of the range in sun angles (Fig. 10), the radiance ratio varies between ~0.85 and 1.15 (i.e. by only ~±15%). The reader is cautioned that this ratio is dependent on the phase function and that for phase functions with a pronounced backward peak the variation near $\theta_0 = 0$ would be stronger than shown in Fig. 10, especially for small ω_0. An investigation of the influence of the phase function on this radiance ratio, however, is beyond the scope of the present study. Thus, to a good approximation, we can take $L_u{}^{\text{true}}(\text{sky})/L_u{}^{\text{true}}(\text{sun}) = 1$, and the radiance error depends only on θ_0 and $E_d(\text{sky})/E_d(\text{sun})$. The

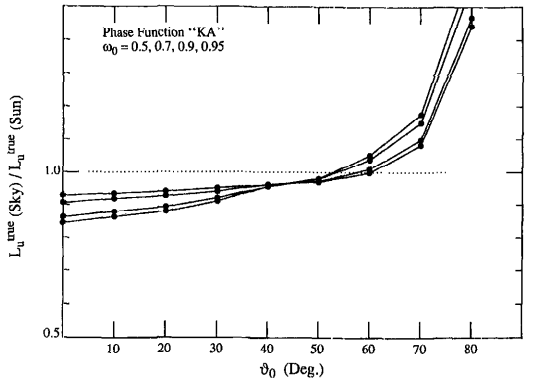

Fig. 10. Sky-sun radiance ratio for use in Eq. 3. Smaller values of ω_0 have larger variation in the ratio with θ_0.

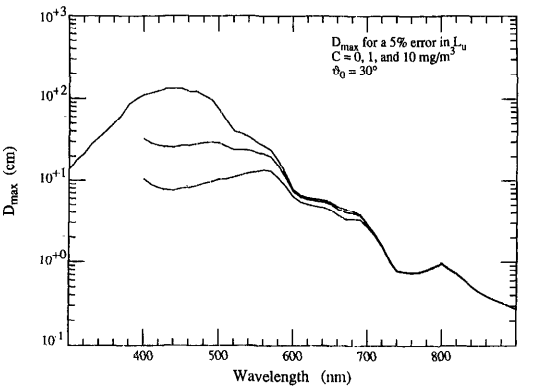

Fig. 11. D_{max} as a function of the pigment concentration C (case 1 waters) such that the error in the *direct* measurement of L_u is $\leq 5\%$. C increases from top to bottom. If corrections are applied as described in the text, D_{max} could be increased by a factor of ~6 and an error $\leq 5\%$ could still be achieved.

procedure for estimating the self-shading-induced error in the radiance when the error is sufficiently small is straightforward: measure $E_d(\text{sky})/E_d(\text{sun})$ with the method described by Gordon (1989); use k' in Table 1 corresponding to the given value of θ_0 in Eq. 2 to estimate $\epsilon(\text{sun})$ in Eq. 3; use k' in Table 3 to estimate $\epsilon(\text{sky})$ in Eq. 3; and estimate a by taking it to be that of pure seawater (a good approximation in the NIR) or by other means, e.g. approximate it by the inherent downwelling irradiance attenuation coefficient just beneath the sea surface (Gordon 1989). For E_u the procedure is the same.

It is instructive to estimate the maximal instrument diameter D_{max} for a given accuracy across the spectrum (Fig. 11). The situation shown in Fig. 11, $\theta_0 = 30°$, is particularly simple since the direct sunlight and skylight errors are almost identical, and no distinction between the two forms of illumination is necessary. In preparing the figure the absorption coefficient is taken to be made up of that due to pure seawater and that due to phytoplankton, i.e. $a = a_w + a_p$. We have taken the absorption coefficient of pure seawater a_w from Smith and Baker (1981) and the absorption coefficient for suspended particles a_p from the model Gordon (1989) utilized, based on the work of Prieur and Sathyendranath (1981) in which a_p is provided in terms of the sum of the concentrations of Chl a and pheophytin a (i.e. the pigment concentration C). The contribution to absorption from other constituents, such as yellow substances, has been ignored, but their effect would be to *reduce* D_{max}, so that D_{max} in Fig. 11 is an *upper* limit.

The curves in Fig. 11 show, for example, that when $D = 10$ cm, the shadow-induced error is $>5\%$ for nearly all wavelengths >600 nm and when $C \gtrsim 10$ mg m^{-1} the error is $>5\%$ for the *entire* spectrum. At high pigment concentrations the computed D_{max} in the 400–500-nm spectral region is *smaller* than many traditional instruments. This result implies that corrections for instrument self-shading should be applied if measurements with $\epsilon < 5\%$ are required. As discussed earlier, D_{max} is < 1 cm in the NIR and independent of C.

Using this graph, it is easy to compute the error as a function of wavelength for an instrument of a given size. Let D be the diameter of the instrument and D_{max} the diameter that produces an error of 5%. Then the error ϵ when the instrument is used is given by

$$\epsilon = 1 - (0.95)^{D/D_{max}}.$$

As an example, we compute ϵ (Fig. 12) for the well-known Scripps spectroradiometer (Tyler and Smith 1966, 1970), for which $D = 35$ cm, operating in the L_u mode (Austin 1980; Tyler and Smith 1967). For this instrument the error is $\lesssim 5\%$ only in the 400–500-nm region and then only for $C < 1$ mg

m^{-1}. Using this instrument (uncorrected) for developing ocean color algorithms (Austin 1980; Clark 1981; Gordon and Clark 1980) would introduce a pigment-dependent error in the ratio of L_u at 440 nm to that at 550 nm ranging from a ratio that is ~4% too high at $C = 0$ to one that is 12% too low at $C = 10$ mg m^{-3}. For wavelengths >600 nm, the error exceeds 20% for all values of C and becomes very large in the NIR.

Clark's (1981) spectroradiometer, which was used to derive the Coastal Zone Color Scanner (CZCS) pigment algorithm, was somewhat larger ($D \approx 42$ cm), leading to even larger errors. Clearly, corrections for self-shading are required for these instruments and for the remote-sensing algorithms derived from them, but the small *bias* introduced by shadowing will likely be less than the inherent "noise" in the algorithms caused by, for example, variations among species. For the situation in Fig. 12, corrections are feasible using the techniques described here as long as $aR \lesssim 0.06$ (Fig. 8), i.e. $a \lesssim 0.12/D = 0.34$ m^{-1}, which is satisfied for wavelengths $\lesssim$650 nm.

The simulations provided in this paper quantify the magnitude of the self-shading of optical radiometers operated just beneath the sea surface and show that typically instruments will require corrections under some conditions. Although a correction technique has been proposed, and its range of validity estimated (Fig. 8), instrument builders are still encouraged to make radiometers as small as feasible to reduce the self-shading error and to allow a less accurate value to be used for the (usually) unknown absorption coefficient required to make the correction. For the NIR, Fig. 8 can be used to estimate the maximal value of D such that, when corrections for self-shading are made, the error in L_u or E_u will be <5%. for L_u the maximal D values are ~2.4 and 1.2 cm at 765 and 865 nm, respectively, for $\theta_0 \geq 20°$, while for E_u, the corresponding values are ~6.4 and 3 cm for $\theta_0 \geq 0$.

Two phenomena that have not been considered in the present computations are surface waves and inelastic processes such as fluorescence and Raman scattering (Marshall and Smith 1990; Stavn and Weidemann 1988). Surface roughness will cause the shadow in Fig. 1 to fill in with *direct* sunlight and decrease the error, but the simulations of Preisendorfer and Mobley (1986) suggest that this effect could be significant only for large values of θ_0 for which the self-shading error is already minimal. The Gordon (1985) code does not consider inelastic processes, so we will use the analytical model described earlier to estimate bounds for the error in their presence. In general, inelastic scattering produces what is believed to be only a small part of the upwelling light field at the sea surface (Stavn 1990). An exception is the in vivo solar-stimulated fluorescence of Chl *a* (Gordon 1979), which often accounts for most of the upwelled light in case 1 waters near 685 nm.

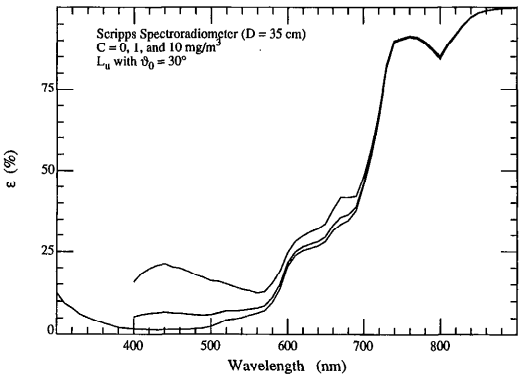

Fig. 12. The error ϵ in the *direct* measurement of L_u at various pigment concentrations for an instrument the size of the Scripps spectroradiometer.

We consider a situation in which L_u is generated *only* by Chl *a* fluorescence, i.e. the absence of *elastic* scattering. Fluorescence is proportional to the number of quanta absorbed by the phytoplankton, which near the surface is proportional to the product of the average (over the spectrum) absorption coefficient and the photosynthetically available radiation (PAR). Since the absorption coefficient of water plus plankton is large in the fluorescence band, one expects of the upwelling fluorescence to vary with depth in a manner similar to the excitation, i.e. PAR. Thus, K_u, the upwelling radiance attenuation coefficient, should be $\approx K$(PAR), the attenuation coefficient for PAR. [For Morel's stations C67 and C71 discussed by Gordon (1979), the observed

upwelling *irradiance* attenuation coefficients at 685 nm were 0.3 and 0.5 m^{-1}, respectively, while the corresponding K(PAR) values were ~0.25 and 0.5 m^{-1}.] With this approximation, the radiance error is given by Eq. 2 with $k = (1 + K(\text{PAR})/a)/\tan\theta_{0w}$, where a is the absorption coefficient of the medium at 685 nm. From Morel (1988) and Kiefer et al. (1989), we estimate that

$$\frac{1}{10} \lesssim \frac{K(\text{PAR})}{a} \lesssim \frac{1}{2},$$

for $0.1 \lesssim C \lesssim 20$ mg m^{-1} (the larger C produces the larger K(PAR)/a). These limits yield $1.1 \lesssim k \tan\theta_{0w} \lesssim 1.5$ for the L_u fluorescence measurement compared to $k \tan\theta_{0w} = 2$ for inelastic scattering. If the error is sufficiently small, then $\epsilon \approx kaR$ and the error in the fluorescence measurement would be ~0.55–0.75 of the error for elastic scattering. Note that this calculation assumes that "filling in" of the instrument shadow in Fig. 1 by scattering is *not* an important factor in reducing ϵ. This assumption holds for $aR \ll 1$ and $\theta_0 > 0$ (Figs. 3, 4).

References

AUSTIN, R. W. 1980. Gulf of Mexico ocean-color surface-truth measurements. Boundary-Layer Meteorol. **18:** 269–285.

CLARK, D. K. 1981. Phytoplankton algorithms for the Nimbus-7 CZCS, p. 227–238. *In* J. R. F. Gower [ed.], Oceanography from space. Plenum.

GORDON, H. R. 1979. The diffuse reflectance of the ocean: The theory of its augmentation by chlorophyll *a* fluorescence at 685 nm. Appl. Opt. **18:** 1161–1166.

———. 1985. Ship perturbation of irradiance measurements at sea. 1: Monte Carlo simulations. Appl. Opt. **23:** 4172–4182.

———. 1989. Can the Lambert-Beer law be applied to the diffuse attenuation coefficient of ocean water? Limnol. Oceanogr. **34:** 1389–1409.

———, O. B. BROWN, AND M. M. JACOBS. 1975. Computed relationships between the inherent and apparent optical properties of a flat homogeneous ocean. Appl. Opt. **14:** 417–427.

———, AND D. K. CLARK. 1980. Atmospheric effects in the remote sensing of phytoplankton pigments. Boundary-Layer Meteorol. **18:** 299–313.

———, AND OTHERS. 1983. Phytoplankton pigment concentrations in the Middle Atlantic Bight: Comparison between ship determinations and Coastal Zone Color Scanner estimates. Appl. Opt. **22:** 20–36.

———, ———, J. L. MUELLER, AND W. A. HOVIS. 1980. Phytoplankton pigments derived from the Nimbus-7 CZCS: Initial comparisons with surface measurements. Science **210:** 63–66.

———, AND A. Y. MOREL. 1983. Remote assessment of ocean color for interpretation of satellite visible imagery: A review. Springer.

HALE, G. M., AND M. R. QUERRY. 1973. Optical constants of water in the 200-nm to 200-μm wavelength region. Appl. Opt. **12:** 555–563.

HOVIS, W. A., AND OTHERS. 1980. Nimbus 7 coastal zone color scanner: System description and initial imagery. Science **210:** 60–63.

KIEFER, D. A., W. S. CHAMBERLIN, AND C. R. BOOTH. 1989. Natural fluorescence of chlorophyll *a*: Relationship to photosynthesis and chlorophyll concentration in the South Pacific gyre. Limnol. Oceanogr. **34:** 868–881.

KULLENBERG, G. 1968. Scattering of light by Sargasso Sea water. Deep-Sea Res. **15:** 423–432.

MARSHALL, B. R., AND R. C. SMITH. 1990. Raman scattering and in-water ocean optical properties. Appl. Opt. **29:** 71–84.

MOREL, A. 1988. Optical modeling of the upper ocean in relation to its biogenous matter content (case 1 waters). J. Geophys. Res. **93:** 10,749–10,768.

———, AND L. PRIEUR. 1977. Analysis of variations in ocean color. Limnol. Oceanogr. **22:** 709–722.

NASA AND THE EARTH OBSERVATIONS SATELLITE CO. 1987. System concept for wide-field-of-view observations of ocean phenomena from space.

PREISENDORFER, R. W. 1961. Application of radiative transfer theory to light measurements in the sea. Int. Union Geod. Geophys. Monogr. 10, p. 11–30.

———, AND C. D. MOBLEY. 1986. Albedos and glitter patterns of a wind-roughened sea surface. J. Phys. Oceanogr. **16:** 1293–1316.

PRIEUR, L., AND S. SATHYENDRANATH. 1981. An optical classification of coastal and oceanic waters based on the specific absorption curves of phytoplankton pigments, dissolved organic matter, and other particulate materials. Limnol. Oceanogr. **26:** 671–689.

SMITH, R. C., AND K. S. BAKER. 1981. Optical properties of the clearest natural waters (220–800 nm). Appl. Opt. **20:** 177–184.

STAVN, R. H. 1990. Raman scattering effects at the shorter visible wavelengths in clear ocean water, p. 94–100. *In* Ocean Optics 10, Proc. SPIE **1302.**

———, AND A. D. WEIDEMANN. 1988. Optical modeling of clear ocean light fields: Raman scattering effects. Appl. Opt. **27:** 4002–4011.

TYLER, J. E., AND R. C. SMITH. 1966. Submersible spectroradiometer. J. Opt. Soc. Am. **56:** 1390–1396.

———, AND ———. 1967. Spectroradiometric characteristics of natural light under water. J. Opt. Soc. Am. **57:** 595–601.

———, AND ———. 1970. Measurements of spectral irradiance underwater. Gordon and Breach.

Submitted: 11 July 1991
Accepted: 29 October 1991
Revised: 19 February 1992